Connecting the Dots: MUSE Unveils the Destructive Effect of Massive Stars

Anna Faye McLeod[1]
Adam Ginsburg[1]
Pamela Klaassen[2]
Joseph Mottram[3]
Suzanne Ramsay[1]
Leonardo Testi[1,4]

[1] ESO
[2] UK Astronomy Technology Centre, Edinburgh, United Kingdom
[3] Max-Planck-Institut für Astronomie, Heidelberg, Germany
[4] INAF Osservatorio di Arcetri, Florence, Italy

Throughout their entire lives, massive stars have a substantial impact on their surroundings, such as via protostellar outflows, stellar winds, ionising radiation and supernovae. Conceptually this is well understood, but the exact role of feedback mechanisms on the global star formation process and the stellar environment, as well as their dependence on the properties of the star-forming regions, are yet to be understood in detail. Observational quantification of the various feedback mechanisms is needed to precisely understand how high mass stars interact with and shape their environment, and which feedback mechanisms dominate under given conditions. We analysed the photo-evaporative effect of ionising radiation from massive stars on their surrounding molecular clouds using MUSE integral field data. This allowed us to determine the mass-loss rate of pillar-like structures (due to photo-evaporation) in different environments, and relate it to the ionising power of nearby massive stars. The resulting correlation is the first observational quantification of the destructive effect of ionising radiation from massive stars.

Pillar-like structures are a ubiquitous feature of massive star-forming regions. The ionising radiation from young and nearby high mass stars is not only responsible for the inflation of H II regions, but also for shaping, compressing and destroying the surrounding molecular clouds. Whether these pillar-like structures form from pre-existing dense structures within the clouds, which are then exposed by stellar feedback, or via gas compression and subsequent instabilities (for example, Gritschneder et al., 2010; Tremblin et al., 2012) is still debated. However, these structures, which typically point back into the HII region towards the feedback-driving massive stars, are seen in both observations and simulations of massive star-forming regions. They are found to lose mass as the ionising radiation to which they are exposed gradually destroys them. This process happens via photo-evaporation, in which the surface layer of the pillar material (composed of dust and molecular gas) is ionised and heated and as a consequence streams away from the pillar surface in a so-called photo-evaporative flow (Hester et al., 1996). This phenomenon was already described with analytical models some twenty years ago (Bertoldi, 1989; Lefloch & Lazareff, 1994), but a quantitative observational test of such models has been lacking so far.

Previous observations of the Pillars of Creation in M16 (McLeod et al., 2015) with the Multi Unit Spectroscopic Explorer (MUSE) demonstrated that the instrument is ideal for the determination of the mass-loss rate from cloud structures due to photo-evaporation, as the simultaneous optical imaging and spectroscopy yield information on both the morphology and kinematics of the ionised evaporating material. The analysis of the M16 pillars was not, however, sufficient to achieve the ultimate goal of determining the connection between the ionising stars and the mass-loss rate due to photo-evaporation. What is needed is a systematic study of pillar-like structures in different star-forming regions, which are subject to different ionising fluxes and are found in different Galactic environments. We obtained such a sample by combining the M16 dataset with MUSE observations of other pillars in the Milky Way — in NGC 3603 and the Carina Nebula Complex. The full analysis is presented in McLeod et al. (2016).

The sample

In order to sample photo-evaporating pillar-like structures in different environments, we combine MUSE data of three different star-forming regions. These regions differ in terms of their massive star content, as well as location within the Galaxy. All of the observed pillars show ionisation fronts at their tips as they are exposed to the radiation from the nearby massive stars (or star clusters).

The M16 pillars are shown in Figure 1 and lie at ~ 2 pc projected distance south-west of the massive star cluster NGC 6611, which contains about 13 O-type stars (Evans et al., 2005). M16 is situated at a distance of about 2 kpc from the Sun. These pillars can be divided into four different structures with different inclinations towards the observer and different distances along the line of sight. By estimating the mass of the photo-evaporative flow from the sulphur emission, we find these structures to have an expected remaining lifetime of about 3 Myr (McLeod et al., 2015).

At a distance of about 6.9 kpc, NGC 3603 is one of the most massive star-forming regions in the Galaxy, and contains over 30 O-type stars (Melena et al., 2008) in a centrally condensed region surrounded by a bright nebula. There are two parsec-scale pillars about 1 pc away from the central cluster. The south-east pillar was observed with MUSE during Science Verification with a single pointing (Figure 2).

The Carina Nebula Complex (CNC), at a distance of 2.3 kpc, is a very rich and well studied star-forming region, which contains several massive young star clusters and is therefore an ideal region for the analysis of feedback from massive stars. We selected four regions containing pillar-like structures from the recent census presented in Hartigan et al. (2015) in the vicinity of the three main clusters of the CNC (Trumpler [Tr] 14, 15 and 16), in order to sample different conditions in the same region.

With about 10 and 18 O-type stars respectively, the younger clusters Tr 14 and 16 are more massive and more luminous than Tr 15, which boasts only 6 O-stars. Of the four regions, shown in Figure 3, R18 lies about 7 pc north-east of Tr 15, R37 about 4.1 pc north-east of Tr 16, and R44 and R45 are located at > 10 pc east of Tr 14 and Tr 16 respectively. This configuration greatly complicates the determination of the main

Figure 1. MUSE RGB composite of the emission of the pillars in M16 (red = [S II], green = Hα, blue = [O III]) from nine pointings covering an area 3 × 3 arcminutes. See McLeod et al. (2015) and ESO Photo Release eso1518.

ionising source for each pillar. However, as discussed below, the identification of the main ionising sources responsible for the photo-evaporation of the single pillars is of great importance and can be tackled by carefully analysing the spatial orientation of the pillars and the locations of their main ionisation fronts.

The sample of photo-evaporating ionised pillars thus consists of a total of ten objects in three different star forming regions, probing a broad range of radiation field conditions. Furthermore, the six pillars in the CNC are found around different massive clusters, therefore sampling different conditions within the same region.

Ionisation from nearby massive stars

The number of ionising photons reaching each pillar can be estimated from assumptions about which stars or star clusters are responsible for the feedback. Furthermore, we assume that the O-type stars dominate in terms of ionising photon flux, and therefore we do not consider the B-type stars. To determine the number of O-stars in each region we refer to population studies from the literature (see below) and convert the spectral types of the known O-stars to a photon flux Q_0 according to Martins et al. (2005). The isotropically emitted photon flux then needs to be scaled to the distance of the feedback-affected pillars, as well as the size of their exposed tips. For this step, we determine the solid angle subtended by the pillar tips with respect to the ionising sources, under the assumption that the pillar tips can be approximated as spherical caps.

In the case of NGC 3603 and M16, which host only one massive cluster each, we assume that the pillars are subject to the combined flux from all the O-stars in the

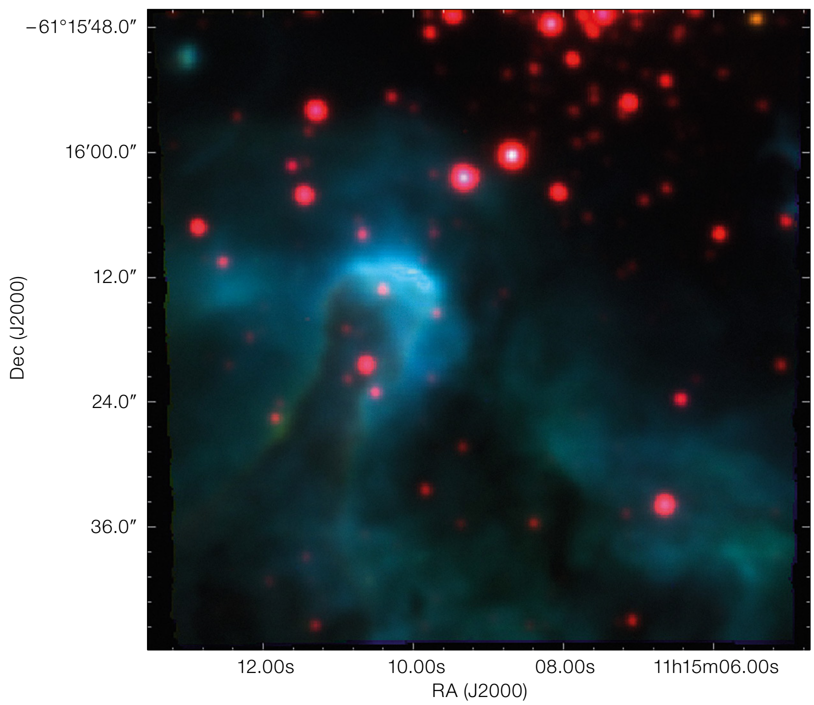

Figure 2. MUSE RGB composite of the pillar in NGC 3603 (same colour coding as Figure 1). The field is 1 × 1 arcminutes (single MUSE pointing).

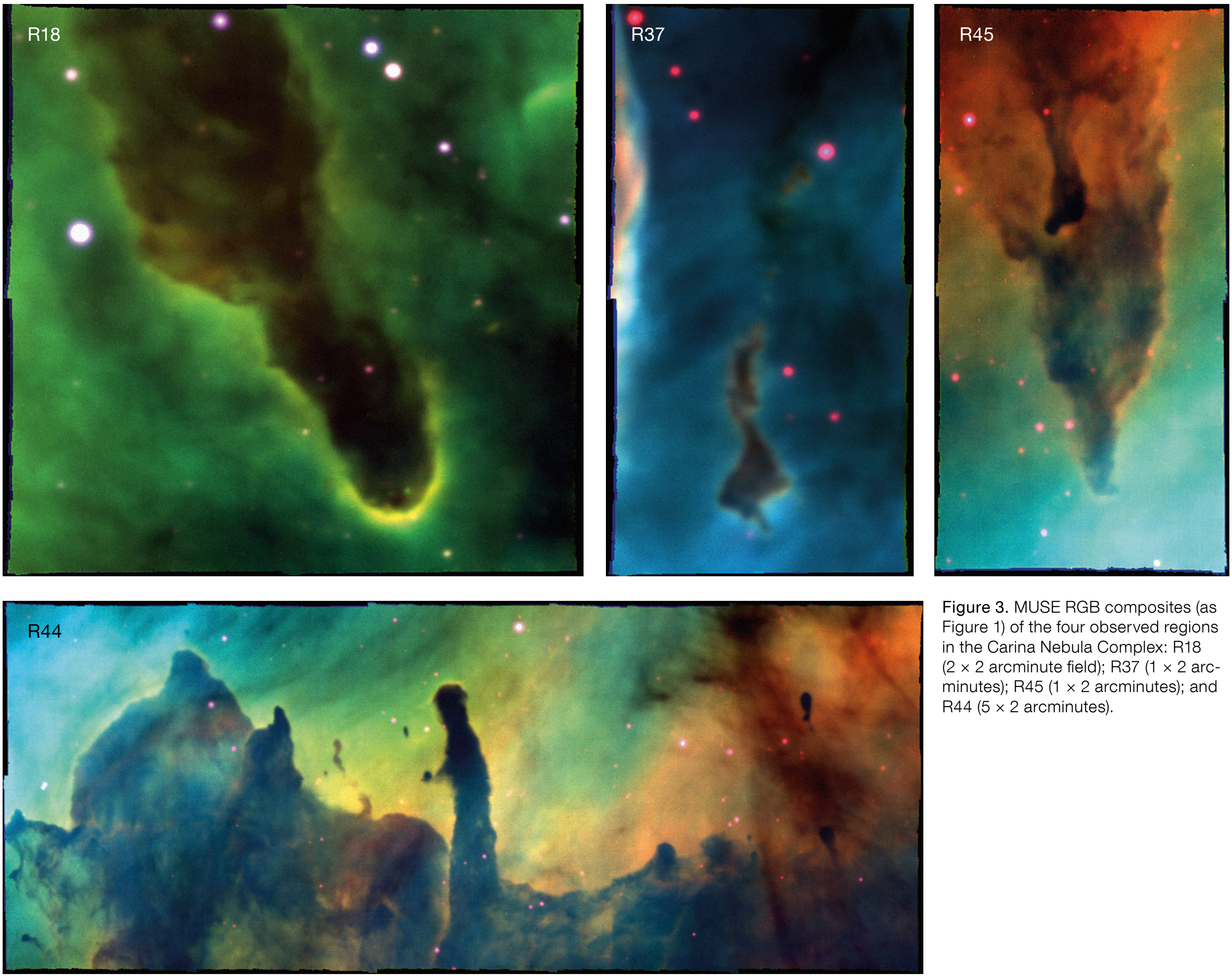

Figure 3. MUSE RGB composites (as Figure 1) of the four observed regions in the Carina Nebula Complex: R18 (2 × 2 arcminute field); R37 (1 × 2 arcminutes); R45 (1 × 2 arcminutes); and R44 (5 × 2 arcminutes).

nearby cluster. For the 33 O-type stars in NGC 3603 (Melena et al., 2008) we estimate log Q_0 ~ 50.98 s^{-1}, while for the 13 O-stars of NGC 6611 (Evans et al., 2005) we calculate log Q_0 ~ 49.87 s^{-1}. We then scale the photon flux Q_0 to the projected distance and size of the ionised pillar tips as described above to obtain the photon flux at the respective pillar tips, $Q_{0,pil}$. Values of $Q_{0,pil}$ can be found in Table 3 of McLeod et al. (2016).

For the pillars in the CNC, where multiple ionising star clusters are present within a few tens of parsecs of each other in the same star-forming region, particular care needs to be taken when determining which O-type stars affect which pillars. We combine the relative projected distances of each pillar in Carina with its orientation and ionisation structure (thus assuming that the orientation of the main pillar body is indicative of the origin of the incident radiation) to determine the ionising sources. The pillar in region 18 (R18 in Figure 3) is closest (~ 7 pc) to Tr 15 and points directly back towards the central coordinates of this cluster; we therefore considered the combined flux of the Tr 15 O-stars.

The globule in R37 is just 4.1 pc north of Tr 16, but points instead at two massive stars away from the cluster centre. These two, an O4 and a Wolf-Rayet star, have a combined photon flux of log Q_0 ~ 50.18 s^{-1}. The pillars in both R44 and R45 lie east of Tr 14 and Tr 16, but their orientation and ionisation fronts do not coincide with direct feedback from either of these clusters. Rather, the pillars in these two regions point in the direction of an O6 and an O9.5 star, which have a combined photon flux of log Q_0 ~ 49.02 s^{-1}.

Computing the mass-loss rate and connecting the dots

Next, we compute the mass-loss rate due to photo-evaporation using the expression given in Smith et al. (2004), which relates the radius of curvature r of the pillar cap, the proton mass m_H, the matter density N_H and the velocity of the ionised photo-evaporative flow ν. In order to compute N_H, we exploit the

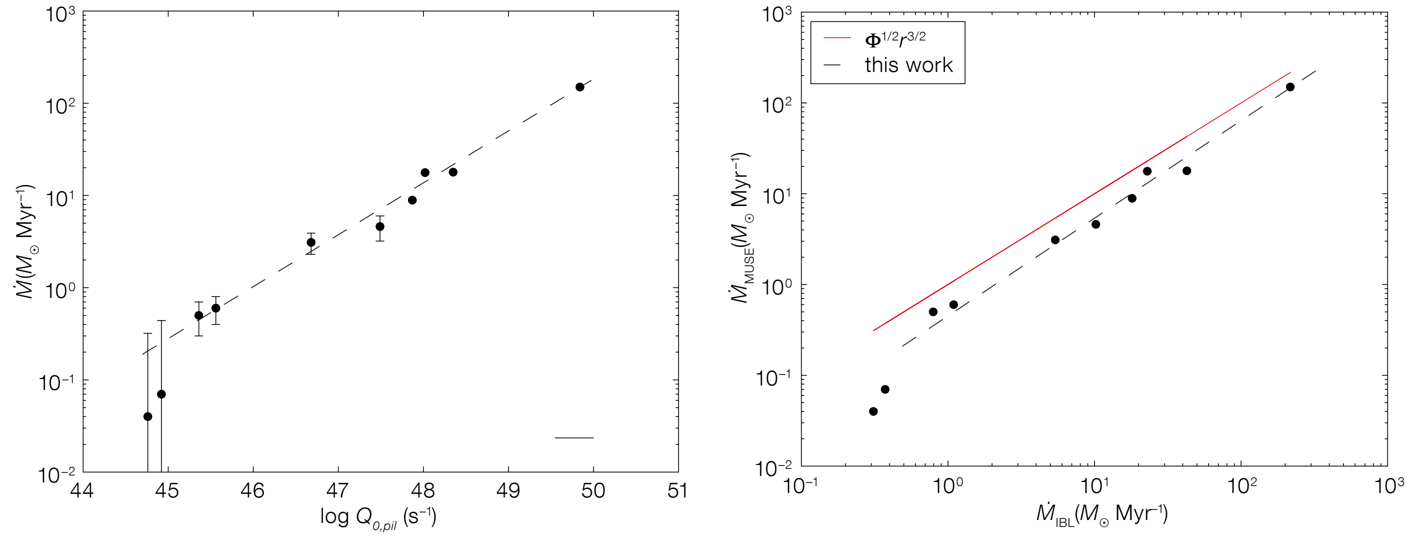

Figure 4. Left: The observed correlation between the ionising photon flux incident at the pillar tips ($Q_{0,pil}$) and the mass loss rate due to photo-evaporation. The dashed line indicates the best fit power law with index $p = 0.56 \pm 0.02$, while the horizontal line indicates the average uncertainty in log $Q_{0,pil}$. Right: The empirically determined correlation (dashed line, this work) compared with the model by Lefloch & Lazareff (1994), indicated by the red line. Here, Φ is the ionising photon flux $Q_{0,pil}$ as scaled in the analytical model. and $\dot{M}_{\mathrm{IBL}}$ the mass loss rate of the ionisation boundary layer (IBL).

MUSE coverage of the sulphur doublet [S II] 6717,6731 Å to produce maps of the electron density N_e (see McLeod et al., 2015), and by converting the value of N_e extracted from a circular aperture at the ionised pillar tips according to $N_e \sim 0.7\ N_H$ (Sankrit & Hester, 2000). The velocity of the ionised photo-evaporative flow is obtained by fitting the stacked spectrum[1] of the main emission lines within ~ 500 Å of the Hα line with a Gaussian fitting routine on a pixel-by-pixel basis, resulting in a velocity map for each region. In the velocity maps (see McLeod et al., 2016), the pillars are clearly distinguishable from the ambient matter, as they appear blueshifted with respect to the latter. The reason for this is that the photo-evaporative flow is normal to the surface of the pillars.

By relating the mass-loss rate computed for each individual pillar to the incident ionising photon flux $Q_{0,pil}$, we obtain a tight correlation between the two as shown in Figure 4 (left panel), which is best fitted with a power law of index $p = 0.56$. This is the first observational test of the analytical models describing photo-evaporation in ionised nebulae (Bertoldi, 1989; Lefloch & Lazareff, 1994), and indicates that objects that are subject to a lower ionising photon flux show lower mass-loss rates and therefore, if they have the same mass, have longer expected lifetimes.

We further compare our empirical result with the theoretical mass-loss rate derived in Lefloch & Lazareff (1994) and

Figure 5. The dependence of the electron density N_e on the ionising photon flux $Q_{0,pil}$ (left panel) and the projected distance, d, to the main ionising sources (right panel).

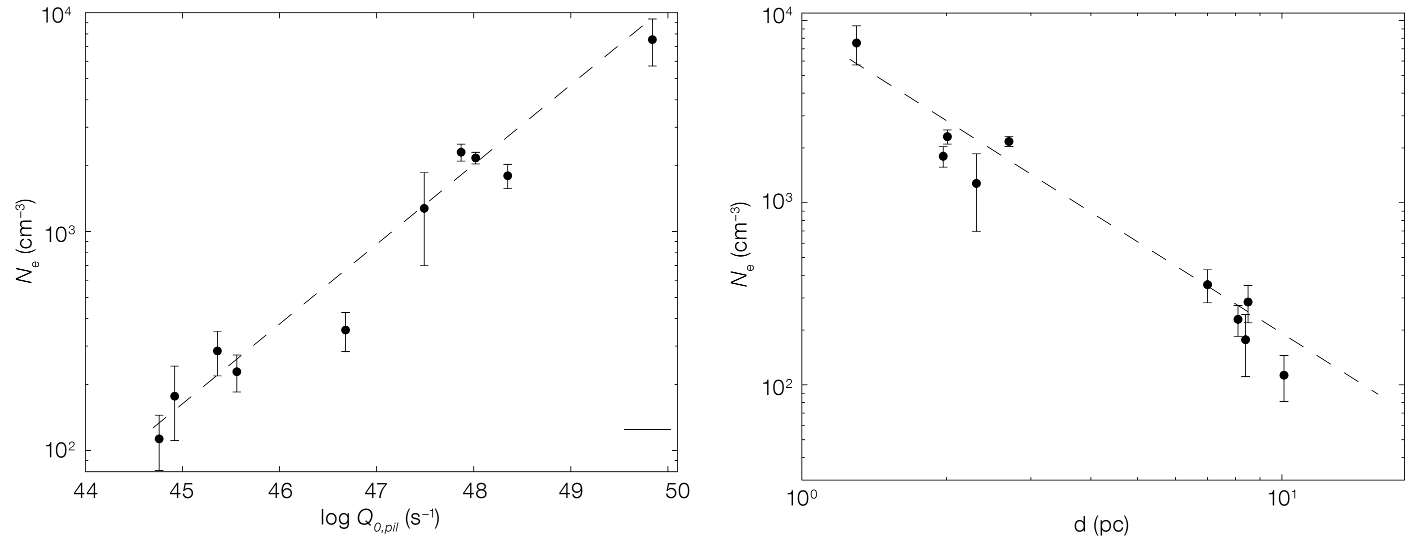

find very good agreement between the observations and the model, in which the mass-loss rate is proportional to $(Q_{0,pil})^{1/2}$ and $r^{3/2}$. The comparison with the model is shown in the right panel of Figure 4, where the mass-loss rates measured with MUSE are plotted against the values found for the so-called ionisation boundary layer (IBL). In the IBL picture, not all of the incident photons lead to ionisation at the pillar tip, as some of them are absorbed in the photo-evaporative flow to compensate recombination. The model and the observations differ by a factor of about two, which can be partly explained by the geometry of the pillar tips assumed for the computation of the mass-loss rate. This intuitively simple picture is, however, further complicated by the empirical dependence of the electron density (used to compute the mass-loss rate) on both the distance and the incident photon flux, as shown in Fig. 5. This dependence is not described by the models with which we compare our findings, and will require further investigation in order to fully disentangle the various dependencies.

These results deliver the first observational quantification of the effect of ionisation from massive stars which can be used to test models of feedback from such stars. This is a crucial step, as feedback from massive star formation represents, to date, one of the main uncertainties in galaxy evolution models, and observational constraints are needed in order to properly understand them and model the important physical mechanisms. The integral field spectrograph MUSE offers the possibility of performing simultaneous morphological and kinematical surveys of feedback-driven structures across different star forming regions. This approach not only yields uniform datasets from the same instrument, but also drastically improves on observations which can be expensive in terms of the necessary telescope time. Furthermore, MUSE also offers the possibility of both analysing the feedback-driven gas and identifying and classifying the feedback-driving massive stars. On account of these advantages, MUSE is an ideal instrument to trace feedback in massive star-forming regions.

References

Bertoldi, F. 1989, ApJ, 346, 735
Evans, C. J. et al. 2005, A&A, 437, 467
Gritschneder, M. et al. 2010, ApJ, 723, 971
Hartigan, P. et al. 2015, AJ, 149, 101
Hester, J. J. et al. 1996, AJ, 111, 2349
Lefloch, B. & Lazareff, B. 1994, A&A, 289, 559
Martins, F. et al. 2005, A&A, 436, 1049
McLeod, A. F. et al. 2015, MNRAS, 450, 1057
McLeod, A. F. et al. 2016, MNRAS, in press, arXiv:1608.00005
Melena, N. W. et al. 2008, AJ, 135, 878
Sankrit, R. & Hester, J. J. 2000, AJ, 535, 847
Smith, N. et al. 2010, MNRAS, 405, 1153
Tremblin, P. et al. 2012, A&A, 538, A31

Notes

[1] This is a necessary step, as the MUSE line spread function is undersampled and we therefore obtain a better sampled spectrum. Specifically, the lines used for this fit are Hα, [S II] 6717,6731 Å, [N II] 6548,6584 Å, [O I] 6300,6363 Å and He I 6678 Å.

Wide field colour composite image, formed from broad-band filters (*B*, *V*, *I*) and narrow-band Hα, of the NGC 3603 Galactic star forming region taken with the MPG/ESO Wide Field Imager (WFI). Release eso1425 gives more information.